Applied Catalysis B: Environmental 184 (2016) 355–363

Contents lists available at ScienceDirect

Applied Catalysis B: Environmental

journal homepage: www.elsevier.com/locate/apcatb

Plasma-catalytic degradation of benzene over Ag–Ce bimetallic oxide catalysts using hybrid surface/packed-bed discharge plasmas

Nan Jiang, Jian Hu, Jie Li*, Kefeng Shang, Na Lu, Yan Wu

Institute of Electro statics and Special Power, School of Electrical Engineering, Dalian University of Technology, Dalian 116024, PR China

ARTICLE INFO

Article history:
Received 12 September 2015
Received in revised form
19 November 2015
Accepted 30 November 2015
Available online 3 December 2015

Keyword:
Plasma-catalysis
Benzene
Hybrid discharge plasmas
Ag–Ce bimetallic catalysts

ABSTRACT

Plasma-assisted catalysis has been employed for the degradation of benzene by hybrid surface/packed-bed discharge (HSPBD) plasmas over a series of Ag_x Ce_{1-x}/γ-Al_2O_3 catalysts in in-plasma catalysis (IPC) and post-plasma catalysis (PPC) configurations. In order to study the influence of catalysts placement on discharge characteristics and the consequent synergetic effect in plasma-catalysis process, the catalysts were introduced inside and downstream the surface discharge region (region I) and packed-bed discharge region (region II), respectively, and the benzene degradation performance was investigated in these systems. The effects of the Ag/Ce molar ratio and water vapor have also been investigated in terms of benzene degradation efficiency and CO_2 selectivity. Compared with the plasma-only process, the combination of plasma with Ag_x Ce_{1-x}/γ-Al_2O_3 catalyst significantly improved the reaction performance, and the combined degradation efficiency is a synergistic effect rather than simply an additive effect. Besides, the emission of discharge products (O_3 and NO_x) and hazardous intermediates (formic acid and CO) was markedly suppressed with the introduction of catalyst. The highest benzene degradation efficiency of 96.2% and CO_2 selectivity of 77.3% can be achieved with $Ag_{0.9}Ce_{0.1}/\gamma$-Al_2O_3 catalyst at the *SIE* of 400 J/L. This result suggests that the interaction between a certain proportion of Ag and Ce species over the catalyst is capable of activating the surface lattice and generating more surface adsorbed oxygen (O_{ads}), which favors the plasma-catalytic oxidation reaction. PPC processes can decompose O_3 and destroy benzene more effectively than IPC processes, especially when the catalyst was introduced downstream the region II. Adding a small amount of water vapor into plasma-catalysis system enhanced the catalyst activity, however, further increased the water vapor caused an obvious negative impact on the catalyst activity.

1. Introduction

Volatile organic compounds (VOCs), especially aromatic hydrocarbons, are typical contaminants emitted from numerous urban and industrial sources. Benzene, one of the most prevalent VOCs, is widely used in manufacturing processes and petroleum-based industries [1,2]. Excessive exposure to VOCs can cause headache, nausea, unconsciousness, and even health effects on the central nervous system, while its presence in air, groundwater, and soil contribute significantly to some environmental problems [3]. Therefore, increasing environmental awareness has motivated research into a highly efficient and economical approach for the abatement of VOCs.

Various methods have been used for VOCs degradation, and an effective method is the conversion of VOCs into non-toxic products (CO_2 and H_2O) via non-thermal plasma (NTP). The great advantage of NTP is the possibility to produce energetic electrons, UV light radiation, and strong electric field at ambient temperature [4–7]. The inelastic collisions between energetic electrons and bulk molecules lead to the production of highly reactive species (e.g., O_2^-, O_2^+, H_3O^+, O_3^-,N_2 $\left(A^3\sum_u^+\right)$), which are capable of breaking the chemical bonds or initiating a series of chemical reactions, leading to the destruction of VOCs molecules [8]. In our previous study, an improved plasma process, which generates hybrid surface/packed-bed discharge plasmas, was proposed and employed for the degradation of benzene, which showed good performance in benzene degradation, mineralization, and energy yield [9]. However, the selectivity towards the desired non-toxic products (CO_2 and H_2O) via complete mineralization is still low by using plasma-only process, and the formation of unwanted discharge products is inevitable.

* Corresponding author. Fax: +86 411 84709869.
E-mail address: lijie@dlut.edu.cn (J. Li).

http://dx.doi.org/10.1016/j.apcatb.2015.11.044
0926-3373/

A more effective use of plasma is by exploiting its potential via the combination with catalysis. The plasma-catalysis process can integrate the advantage of the quick response from plasma and high selectivity of desired products from catalysis [10]. Furthermore, the development of a suitable catalyst is helpful to eliminate discharge products such as O_3 and NO_x. The plasma can be coupled with catalysis in two different configurations depending on the location of catalysts: in plasma-catalysis (IPC), where the catalysts are placed in the discharge reactor, and post plasma-catalysis (PPC), where the catalysts are placed downstream the discharge reactor [11,12]. In IPC system, the presence of catalysts in NTP may affect the discharge type or induce a shift in the distribution of energetic electrons, and these processes will affect the formation of active species as well as pollutants degradation. In PPC system, the catalysts cannot be activated by plasma generated active species and only long-lived species (e.g., O_3) can react on the catalytic sites. Some highly active species such as molecular and atomic oxygen can be generated from the catalytic ozone decomposition [13–15]. Previous studies have shown that both IPC and PPC processes can lead to an increase of the energy efficiency and CO_2 selectivity compared to plasma-only process, showing its promising potential for VOCs degradation [16]. And a synergistic effect has also been reported in some cases for the degradation of gaseous pollutants, where the performance of plasma-catalysis process is better than the sum of plasma and catalysis alone [17–19]. However, reports on plasma-catalysis in both IPC and PPC systems mainly focused on exploring the enhancement of the degradation efficiency and energy yield, few studies have been conducted on the detailed understanding of the relationship between plasma-catalysis interactions from both a physical and chemical perspective and the synergistic effect occurred under different plasma-catalysis processes.

Different types of catalysts, including supported noble metals (Au, Ag, Pd, and Pt) and transition metals (Mn, Ce, Co, and Ni) have been studied for VOCs degradation in IPC and PPC configurations [20–24]. In recent years, the synthesis and application of bimetallic materials have attracted considerable attention due to their prominent catalytic activity and multiple functionalities. The bimetallic catalysts could achieve chemical transformations which are unprecedented with monometallic catalysts because each component of the catalysts has a particular function in the overall reaction mechanism [25,26]. In some previous work, Ag-based catalysts have been widely used in VOCs degradation due to their good catalytic performance and physical stability at moderate temperature [27,28]. Cerium oxide (CeO_2) has been identified as a heterogeneous oxidation catalyst and exhibited remarkable catalytic activity for gaseous pollutants degradation due to its excellent oxygen storage capacity (OSC) and redox properties between Ce^{4+} and Ce^{3+} [29,30]. Ag–Ce bimetallic catalysts have been regarded as promising catalysts for VOCs degradation due to strong catalytic reduction reaction between Ag and Ce species. Ding et al. [31] reported that the presence of Ag/CeO_2 catalysts in a dielectric barrier discharge (DBD) significantly enhanced the benzene degradation efficiency and CO_2 selectivity, which might be attributed to the formation of plasma-facilitated catalytic redox cycles between Ag and Ce species. For $Ag–CeO_2$ catalyst, Yamazaki et al. [32] reported that adsorbed oxygen species on the Ag surface transfer to the CeO_2 surface through the Ag/CeO_2 interface to form O_n^{x-} species, and exhibited exceptional catalytic performance for soot oxidation below 300 °C. However, up until now, the combination of supported Ag–Ce bimetallic oxide catalysts with NTP for VOCs degradation has not been reported yet. In addition, it is not clear how the interaction between Ag and Ce species will affect the plasma-catalytic oxidation reactions.

In the present work, a hybrid surface/packed-bed discharge (HSPBD) reactor was used to generate plasma. The simultaneous surface discharge and packed-bed discharge were generated and the sequential degradation processing was successfully performed in the HSPBD reactor. A series of $Ag_x Ce_{1-x}/\gamma\text{-}Al_2O_3$ catalysts with different Ag/Ce molar ratios have been prepared by incipient wetness impregnation, which were placed inside and downstream the surface and packed-bed discharge regions, respectively, to construct different plasma-catalysis systems. The effects of Ag/Ce molar ratio, catalyst placement, and water vapor on catalyst activity towards benzene degradation and mineralization were discussed to get a better understanding of the synergistic effect due to the combination of plasma and catalysis.

2. Experimental

2.1. Experimental set-up

Fig. 1 shows a schematic diagram of the experimental set-up. NTP was produced by a hybrid surface/packed-bed discharge (HSPBD) reactor at ambient temperature, as described in detail in our previous works [9]. The HSPBD reactor was made of a plexiglass cylinder (i.d. 35 mm) with a quartz tube (i.d. 13 mm) fixed along its axis as the dielectric barrier. A stainless-steel wire (o.d. 1 mm) coiled around the inner surface of the quartz tube was used as the inner electrode, while a stainless-steel mesh wrapped around the inner surface of the reactor served as the outer electrode. The open area between the quartz tube and the outer electrode was filled with glass beads (3 ± 0.3 mm). As a result, the effective discharge length and packed-bed discharge gap were 190 mm and 9 mm, respectively. When the AC voltage at a frequency of

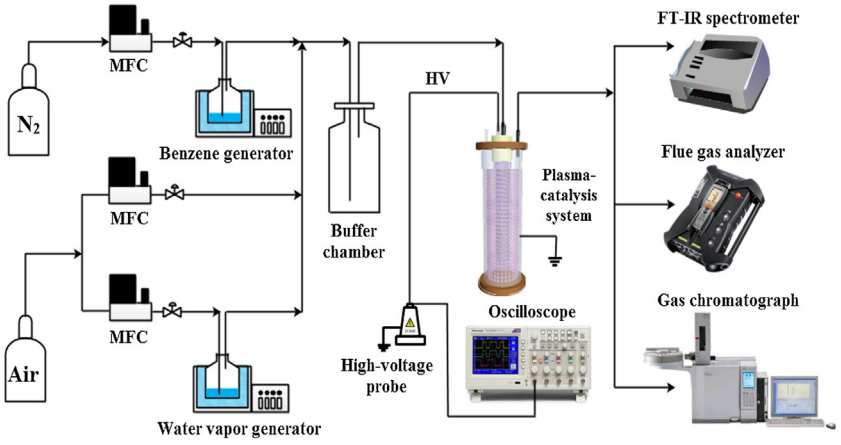

Fig. 1. Schematic diagram of the experimental setup.

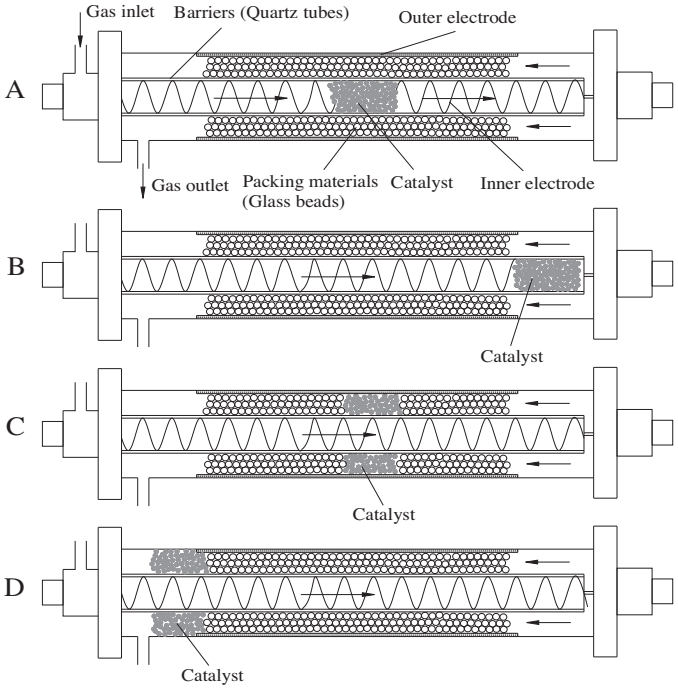

Fig. 2. Different plasma-catalysis systems in IPC and PPC configurations: (a) catalysts were placed in the region I, (b) catalysts were placed downstream the region I, (c) catalysts were placed in the region II, (d) catalysts were placed downstream the region II.

50 Hz is applied between the electrodes, surface discharge starts from the peripheral edges of the inner electrode and stretches out along the dielectric barrier surface, which is defined as the surface discharge region (region I). Simultaneously, a large amount of microdischarges generates at the contact points between the glass beads, which is defined as the packed-bed discharge region (region II). The stimulated gas traverses region I and region II in turn to be treated.

Four plasma-catalysis systems were established to understand the influence of catalyst location on plasma-catalysis reaction and the subsequent degradation performance (Fig. 2). Systems A and C are termed as the IPC systems, where 3 g Ag_x Ce_{1-x}/γ-Al_2O_3 catalysts were packed inside the region I and region II, respectively. The catalyst pellets were held by cotton wool and the height of the catalyst bed was approximately 2 mm. In systems B and D, 3 g Ag_x Ce_{1-x}/γ-Al_2O_3 catalyst was placed downstream the region I and region II, respectively, to compose the PPC systems. The IPC and PPC systems were operated at atmospheric pressure and room temperature.

Reaction gas containing benzene and a certain amount of water vapor was prepared by passing synthetic air (80% nitrogen and 20% oxygen) through two temperature-controlled bubble towers, containing liquid benzene and water, respectively. The initial benzene concentration and gas flow rate were monitored by mass flow controllers (MFC) and fixed at ~400 ppmv and 0.5 L/min, respectively. The gas relative humidity can be adjusted by changing the temperature of the water bubble tower. A gas chromatograph (Shimadzu GC-2010) equipped with a flame ionization detector (FID) was used to analyze the concentration of benzene. CO_2 and CO were quantified using a gas chromatograph (SRI-8610C), equipped with a FID and a methane conversion furnace (GS-101A). The NO_x concentration was measured by a flue gas analyzer (Testo350, Germany), and the quantification of ozone in the DBD reactor was performed by iodometry. The gaseous products were analyzed online using a FT-IR (Nicolet 6700), equipped with a DTGS detector and a 2.4 m gas cell. Spectra were acquired in the wave numbers ranging from 700 to 4000 cm^{-1} with a resolution of 0.5 cm^{-1}. The organic intermediates deposited on the catalyst surface were extracted with *n*-hexane solution (Chromatographic Grade) under ultrasonic vibration for 2 h. The supernatant was filtered with a 0.22 μL filter membrane and analyzed by a GC–MS (Agilent 6980GC-5973MSD) equipped with HP-5MS 30 m × 0.25 mm ID capillary column. The gas temperature in the center of the HSPBD reactor was measured using a fiber optical thermometer (Omega, FOB102). The benzene degradation efficiency ($\eta_{benzene}$), the selectivities of CO, CO_2, and CO_x (S_{co}, S_{co_2} and S_{co_x}) were defined as:

$$\eta_{benzene}(\%) = \left(\frac{C_{in} - C_{out}}{C_{in}}\right) \times 100 \quad (1)$$

$$S_{CO}(\%) = \frac{C_{CO}}{6 \times (C_{in} - C_{out})} \times 100 \quad (2)$$

$$S_{CO_2}(\%) = \frac{C_{CO_2}}{6 \times (C_{in} - C_{out})} \times 100 \quad (3)$$

$$S_{CO_x}(\%) = S_{co} + S_{co_2} \quad (4)$$

where C_{in} and C_{out} are the inlet and outlet concentrations of benzene, respectively. C_{CO} and C_{CO2} are the concentrations of CO and CO_2 excluded from the atmospheric CO_2 at the exit of the reactor, respectively.

2.4. Electrical measurements

All the electrical signals were recorded by a four-channel digital oscilloscope (Tektronix TDS2024). The applied voltage was measured by a high voltage probe (Tektronix EP-50K 5054), and the applied current was recorded by a current probe (Tektronix A6021). The discharge input power was calculated by the voltage-charge (*V*–*Q*) Lissajous figure [33]. The specific input energy (*SIE*) was defined as follows [34]:

$$SIE(J/L) = \frac{P}{Q} \times 60 \quad (5)$$

where *P* is the power dissipated in the discharge (W), *Q* is the gas flow rate through the discharge reactor.

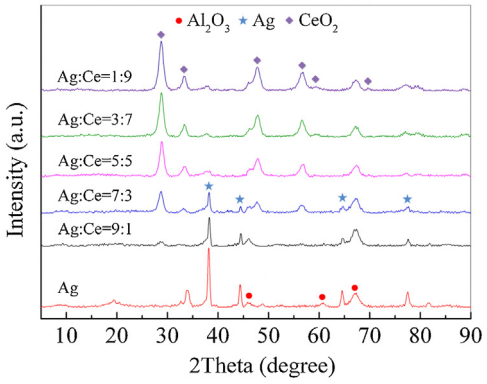

Fig. 3. XRD patterns of the Ag_x Ce_{1-x}/γ-Al_2O_3 catalysts with different Ag/Ce molar ratios.

2.5. Catalyst preparation and characterization

A series of Ag–Ce bimetallic oxide catalysts with different Ag/Ce molar ratios were synthesized by incipient wetness impregnation with γ-Al_2O_3 and aqueous solutions of $AgNO_3$ and $Ce(NO_3)_2$. The impregnated catalysts were first dried at 100 °C overnight and then calcined at 500 °C for 4 h in air flow. After that, the samples were labeled as Ag_x Ce_{1-x}/γ-Al_2O_3, where x represents the molar ratios of Ag to all metal components (Ag + Ce) and equals to 0.9, 0.7, 0.5, 0.3, and 0.1, respectively. For comparison, pure silver oxide was also prepared using a similar procedure. The loading of all metal components was 15%. Gas hourly specific velocity (GHSV), which was calculated based on the gas residence time in the void of the catalyst bed, was 14285 h^{-1} in this study.

The X-ray diffraction (XRD) patterns of catalyst samples were recorded using a Rigaku D/Max-2400 diffractometer equipped with a Cu Kα radiation operated at 40 kV and 40 mA in the 2θ range from 20 to 90°. X-ray photoelectron spectroscopy (XPS) was performed using a ThermoVG ESCALAN250 spectrometer fitted with a monochromatic Al source. All the blinding energies were calibrated to the C1s neutral carbon peak at 284.6 eV. XPS data were analyzed by using the XPS Peak 4.1 software.

3. Result and discussion

3.1. Characterization of the catalysts

3.1.1. XRD results

Fig. 3 shows the XRD patterns of Ag/γ-Al_2O_3 and Ag_x Ce_{1-x}/γ-Al_2O_3 catalysts with different Ag/Ce atomic ratios. All the catalysts show reflections at 2θ of 46.0°, 60.7° and 67°, which are characteristics for the γ-Al_2O_3 phase (cubic defective spinel) [35]. Sharp reflections at 2θ of 38.2°, 44.4°, 64.4° and 77.1° appear besides the γ-Al_2O_3 phase reflection for Ag/γ-Al_2O_3, $Ag_{0.9}Ce_{0.1}$/γ-Al_2O_3 and $Ag_{0.7}Ce_{0.3}$/γ-Al_2O_3, which can be attributed to metallic Ag particles (JCPDS file NO. 65-2871) [36]. However, these reflections are very weak for $Ag_{0.5}Ce_{0.5}$/γ-Al_2O_3, $Ag_{0.3}Ce_{0.7}$/γ-Al_2O_3, and $Ag_{0.1}Ce_{0.9}$/γ-Al_2O_3 catalysts, which indicate their high dispersion or low crystallinity degree over catalysts making it non-detectable with the XRD technique. For Ag_x Ce_{1-x}/γ-Al_2O_3 catalysts, the diffraction peaks can be clearly identified at 2θ of 28.5°, 33.0°, 47.4°, 56.3° and 69.6°, assigned to the (1 1 1), (2 0 0), (2 2 0), (3 1 1) and (4 0 0) lattice planes of the cubic fluorite structure of CeO_2 (JCPDS file NO. 34-0394) [37]. No other peaks related to Ce_2O_3 and $CeAlO_3$ are observed from the XRD patterns.

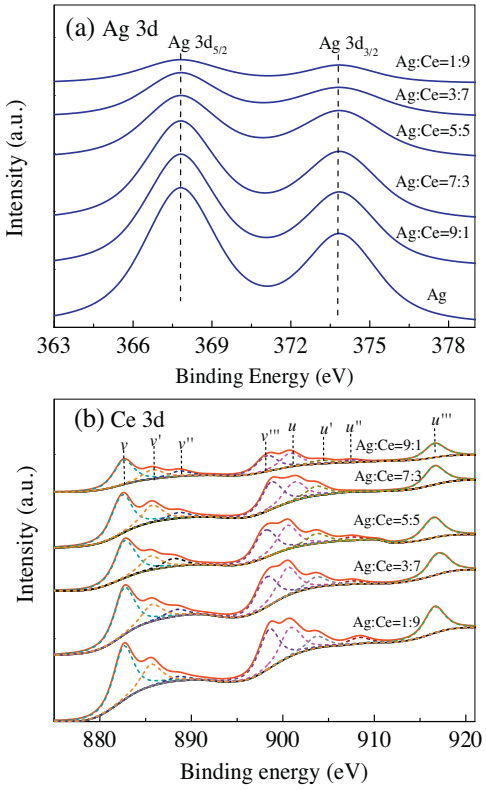

Fig. 4. XPS spectra of the Ag_x Ce_{1-x}/γ-Al_2O_3 catalysts with different Ag/Ce molar ratios: (a) Ag 3d and (b) Ce 3d.

Table 1
Surface Ce element compositions of different Ag_x Ce_{1-x}/γ-Al_2O_3 catalysts.

Catalyst	Ce 3d		
	Surface Ce^{3+} (%)	Surface Ce^{4+} (%)	Ce^{3+}/Ce^{4+} molar ratio
$Ag_{0.9}Ce_{0.1}$/γ-Al_2O_3	18.2	81.8	0.222
$Ag_{0.7}Ce_{0.3}$/γ-Al_2O_3	19.3	80.7	0.239
$Ag_{0.5}Ce_{0.5}$/γ-Al_2O_3	16.6	83.4	0.199
$Ag_{0.3}Ce_{0.7}$/γ-Al_2O_3	16.4	83.6	0.196
$Ag_{0.1}Ce_{0.9}$/γ-Al_2O_3	14.6	85.4	0.171

3.1.2. XPS results

XPS spectra of the Ag_x Ce_{1-x}/γ-Al_2O_3 catalysts with different Ag/Ce molar ratios have been examined to understand the elemental composition of surface and subsurface layers, and the results are shown in Fig. 4.

The Ag 3d spectra of all samples are symmetric and with similar full-width at half-maximum (FWHM), which consisted of two individual peaks at binding energy of 367.7 and 373.8 eV, ascribed to Ag 3d 5/2 and Ag 3d 3/2, respectively. The band at 367.8 eV is attributed to the metallic Ag^0 and that at 373.8 eV is ascribed to the ionic Ag^+ [38]. These results verify the existence of metallic Ag^0 in Ag_x Ce_{1-x}/γ-Al_2O_3 catalysts according to the XRD result.

The XPS spectra of Ce 3d for Ag_x Ce_{1-x}/γ-Al_2O_3 catalysts are represented in Fig. 4(b), where U and V indicate the spin-orbit coupling $3d_{3/2}$ and $3d_{5/2}$, respectively. XPS peaks labeled as v (883.3 eV), v'' (889.2 eV), v''' (898.2 eV), u (901.0 eV), u'' (907.5 eV), and u''' (916.6 eV) correspond to the $3d^{10}4f^0$ state of Ce^{4+} species, whereas the peaks marked as v' (885.7 eV) and u' (903.7 eV) are assigned to the the $3d^{10}4f^1$ state of Ce^{3+} [39]. All the samples analyzed contain predominantly surface Ce^{4+}, with different quantity of Ce^{3+} depending on different Ag/Ce atomic ratios. The surface relative molar ratio of Ce^{3+}/Ce^{4+} is calculated from the curve-fitted Ce 3d spectra [40], and the results are shown in Table 1. It is found that the

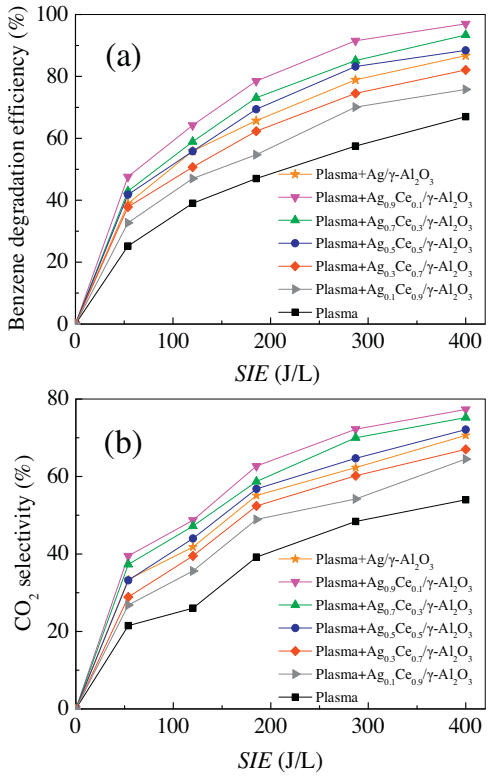

Fig. 5. Effect of $Ag_x Ce_{1-x}/\gamma\text{-}Al_2O_3$ catalysts with different Ag/Ce molar ratios on (a) benzene degradation efficiency and (b) CO_2 selectivity as a function of *SIE*. Condition: the catalyst was placed downstream the region II, gas relative humidity was 0%.

$Ag_x Ce_{1-x}/\gamma\text{-}Al_2O_3$ catalysts with Ag/Ce atomic ratios of 9:1 and 7:3 have higher Ce^{3+}/Ce^{4+} ratio compared to other catalysts, suggesting that a stronger interaction effect occurs between Ag and Ce species in $Ag_x Ce_{1-x}/\gamma\text{-}Al_2O_3$ catalysts with high Ag/Ce atomic ratio. It has already been demonstrated that higher molar ratio of Ce^{3+}/Ce^{4+} favors the formation of surface oxygen vacancies and unsaturated chemical bonds, which will lead to an increase of adsorbed oxygen (O_{ads}) on the catalyst surface [41].

3.2. Effect of Ag/Ce molar ratio on the activity of $Ag_xCe_{1-x}/\gamma\text{-}Al_2O_3$ catalyst

Fig. 5 shows the effect of Ag/Ce molar ratio on the degradation of benzene and CO_2 selectivity as a function of *SIE* in PPC system (system D), and the results are compared with those in NTP system. The benzene degradation efficiency increases with increasing the *SIE* regardless of the catalyst used. Increasing the *SIE* by raising the applied voltage is expected to effectively enhance the reduced electric field and generate more energetic electrons and active species which are capable of initiating a series of chemical reactions. Taking the $Ag_{0.9}Ce_{0.1}/\gamma\text{-}Al_2O_3$ catalyst for example, increasing the applied voltage from 17 to 25 kV significantly increases the *SIE* from 54 to 400 J/L, and consequently enhances the benzene degradation efficiency from 47.6 to 96.2%. The gas temperature in plasma has also been measured in the HSPBD reactor at a *SIE* of 400 J/L. Clearly, the plasma gas temperature increased from 25 to 44 °C in the first 35 min after igniting the plasma, and which grew slowly and retained approximately constant at 46 °C after 45 min discharge treatment, indicating that no thermal chemical reactions occurred.

In comparison to the plasma-only process, the combination of plasma with the $Ag_x Ce_{1-x}/\gamma\text{-}Al_2O_3$ catalyst significantly improves the reaction performance. It can also be observed that no benzene degradation occurs with catalyst alone, suggesting that discharge plasma is indispensable for benzene degradation since the $Ag_x Ce_{1-x}/\gamma\text{-}Al_2O_3$ catalyst cannot be activated without discharge at room temperature. Obviously, the combination of plasma and $Ag_x Ce_{1-x}/\gamma\text{-}Al_2O_3$ shows an unambiguous synergistic effect in benzene degradation and mineralization, rather than a simple additive effect of plasma and catalysis processes. The prominent synergistic effect can be attributed to the efficiency of $Ag_x Ce_{1-x}/\gamma\text{-}Al_2O_3$ catalyst to decompose ozone catalytically. This reaction enables the supply of active oxygen species that assist the destruction of remaining benzene and intermediates exiting the discharge reactor [16]. Therefore, the plasma-catalysis process plays two major roles: to generate additional active species without injecting more energy or to recover the energy wasted in atomic oxygen formation that mainly recombine to produce O_3. In addition, it should be noted that the thermal catalytic activation of benzene can be ignored due to relatively low temperature plasma process used in this study.

It is also seen that adding small amount of Ce into $Ag/\gamma\text{-}Al_2O_3$ catalyst significantly improves the catalyst activity towards benzene degradation and mineralization, which decreases in accordance with this sequence: $Ag_{0.9}Ce_{0.1}/\gamma\text{-}Al_2O_3 > Ag_{0.7}Ce_{0.3}/\gamma\text{-}Al_2O_3 > Ag_{0.5}Ce_{0.5}/\gamma\text{-}Al_2O_3 > AgCe/\gamma\text{-}Al_2O_3 > Ag_{0.3}Ce_{0.7}/\gamma\text{-}Al_2O_3 > Ag_{0.1}Ce_{0.9}/\gamma\text{-}Al_2O_3$ at identical *SIE*. At 400 J/L, 96.2% of benzene was degraded over $Ag_{0.9}Ce_{0.1}/\gamma\text{-}Al_2O_3$ catalyst and the corresponding CO_2 selectivity was 77.3%, which were 9.3% and 6.8% higher, respectively, than those over $Ag/\gamma\text{-}Al_2O_3$ catalyst. However, when the Ag/Ce molar ratio further decreased to 1/9, the benzene degradation efficiency and CO_2 selectivity decreased to only 75.8% and 64.8%, respectively. These results suggest that the interactions between Ag and Ce species could change the catalyst activity, and consequently improve the performance of the plasma-catalytic degradation of benzene. The Ag species in $Ag_x Ce_{1-x}/\gamma\text{-}Al_2O_3$ catalysts are the main active components for benzene oxidation because ozone can be effectively decomposed over Ag catalyst and the catalyst deactivation can be suppressed under mild conditions. Subsequently, the reoxidation of Ag is readily accomplished by the transfer of adsorbed oxygen or the lattice oxygen from CeO_2, which suggests Ce^{4+} serves as an oxygen reservoir and maintains Ag in the oxidized state. The consumed oxygen species on the catalysts can be replenished by gas phase oxygen and active oxygen species generated in the plasma process. CeO_2 acted as a reservoir for the storage and release of oxygen as a result of redox cycle between Ce^{4+} and Ce^{3+} in the $Ag_x Ce_{1-x}/\gamma\text{-}Al_2O_3$ catalysts. The presence of Ce^{3+} on the catalyst surface is capable of activating the surface lattice and facilitating the formation of oxygen vacancies as well as surface adsorbed oxygen species (O_{ads}). Higher concentration of O_{ads} tends to generate more active oxygen species, which could result in higher degradation efficiency of benzene through the surface reactions [42]. The Ce^{3+} relative concentration in the $Ag_{0.9}Ce_{0.1}/\gamma\text{-}Al_2O_3$ and $Ag_{0.7}Ce_{0.3}/\gamma\text{-}Al_2O_3$ catalysts are found to be much higher than that of the other catalysts, which substantially matches the reaction performance of the plasma-catalytic process. Therefore, adding a small amount of Ce into $Ag/\gamma\text{-}Al_2O_3$ catalyst could improve the catalytic degradation of benzene.

3.3. Effect of catalyst placement on degradation reaction performance

3.3.1. Catalytic activity evaluation

In IPC configuration, plasma-catalysis process may facilitate the electron and photon induced processes, change the discharge characteristic and generate active species which can participate in degradation reaction. Whereas in PPC configuration, only long-lived species (such as O_3) and some stable organic intermediates generated by discharge plasma would be involved in plasma-

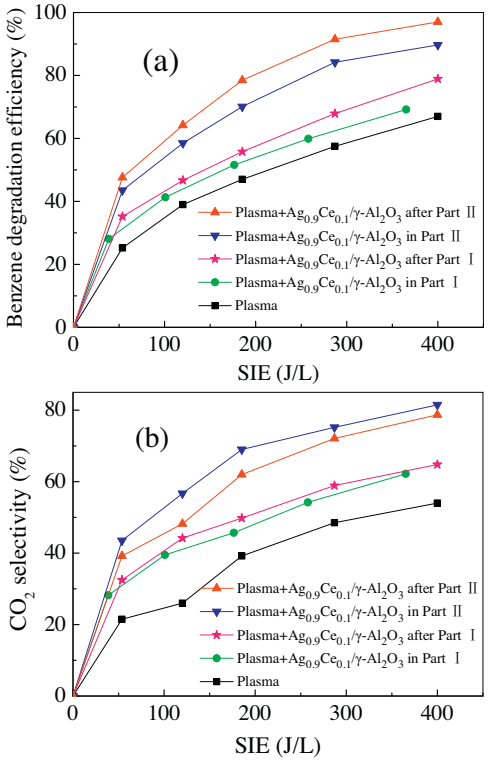

Fig. 6. Effect of plasma-catalysis configurations on (a) benzene degradation efficiency and (b) CO_2 selectivity as a function of *SIE*. Condition: $Ag_{0.9}Ce_{0.1}/\gamma\text{-}Al_2O_3$ was used as the catalyst, gas relative humidity was 0%.

catalytic surface reactions. Therefore, the origin of plasma-catalytic reactions is different depending on the catalyst location respective to the discharge region. Fig. 6(a) shows the benzene degradation efficiency as a function of *SIE* in different plasma-catalysis systems over $Ag_{0.9}Ce_{0.1}/\gamma\text{-}Al_2O_3$ catalysts. The results shows that benzene degradation is strongly affected by the catalyst location in plasma-catalysis reaction, and PPC processes destroy benzene more effectively than IPC processes. Approximately 95.3% and 75.6% of benzene were degraded when the catalysts was placed downstream the region II (system D) and region I (system B) at 366 J/L, which were 7.4% and 6.7% higher, respectively, than the benzene degradation efficiency when the catalysts was introduced inside the region II (system C) and region I (system A). As mentioned previously, ozone decomposition on catalyst surface plays a vital role to induce the performance enhancement mechanism in plasma-catalysis system. Therefore, higher degradation efficiency obtained in PPC processes may be related to their efficiency to catalytically decompose ozone.

Fig. 6(b) presents the CO_2 selectivity as a function of *SIE* in different plasma-catalysis systems with $Ag_{0.9}Ce_{0.1}/\gamma\text{-}Al_2O_3$ catalyst. The result shows that higher CO_2 selectivity can be achieved in system C than system D at the same *SIE*. At 366 J/L, the CO_2 selectivity was 79.6% when the $Ag_{0.9}Ce_{0.1}/\gamma\text{-}Al_2O_3$ catalyst was introduced into the region II (system C), which was 27.2% higher than that in plasma system without catalyst. In system C, the catalyst can prolong gas residence time and increase the concentration of organic intermediates in plasma due to its significant adsorption capacity, which could improve the mineralization efficiency due to higher collision probability between the intermediates and active species. Ogata et al. [43] also found that packing the zeolite (MS-13X) pellets into the ferroelectric packed-bed discharge region is conductive to improving CO_2 selectivity.

In addition, it is interesting to find that packing the catalyst support ($\gamma\text{-}Al_2O_3$) into the region II has little impact on benzene

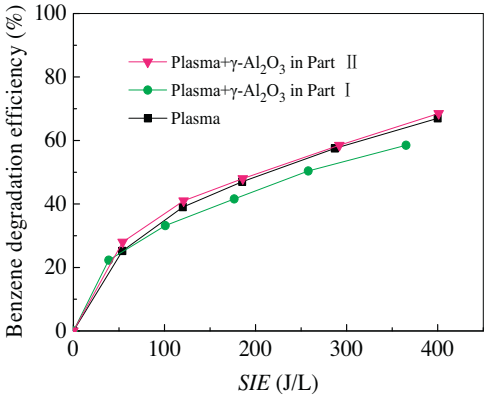

Fig. 7. Effect of the placement of catalyst support ($\gamma\text{-}Al_2O_3$) on benzene degradation as a function of *SIE*. Condition: gas relative humidity was 0%.

degradation. However, packing $\gamma\text{-}Al_2O_3$ into the region I leads to an obvious decrease in benzene degradation compared to plasma-only process (Fig. 7). That is because packing the catalyst pellets into the packed-bed discharge gap can't change the discharge mode greatly, which still exhibits intensive microdischarges at the contact points between the glass beads (or catalyst pellets) due to large packed-bed discharge gap. However, packing the catalyst pellets into the narrow surface discharge gap causes a significant transition in discharge mode from a typical surface discharge to a combination of limited surface discharge and spatially microdischarge between the catalyst pellets. Similar result was also reported by Tu et al. [44], they found that fully packing the catalyst into 3 mm discharge gap suppresses the filamentary discharge and induces a dramatic decrease in CH_4 conversion compared with plasma alone.

3.3.2. Ozone and NO_x production

Formation of O_3 and nitrogen oxides (NO and NO_2) is unavoidable during the discharge, which are also serious air pollutants. Fig. 8(a),(b) shows the concentration of O_3 and NO_2 as a function of *SIE* in different plasma-catalysis systems with $Ag_{0.9}Ce_{0.1}/\gamma\text{-}Al_2O_3$ catalyst, respectively. For plasma-only or plasma-catalysis processes, O_3 and NO_2 concentration increased with the increase of *SIE*. The presence of $Ag_{0.9}Ce_{0.1}/\gamma\text{-}Al_2O_3$ catalyst resulted in a significant decrease in O_3 and NO_2 concentrations, and the decrease was more pronounced with $Ag_{0.9}Ce_{0.1}/\gamma\text{-}Al_2O_3$ catalyst packing after the region II. When the $Ag_{0.9}Ce_{0.1}/\gamma\text{-}Al_2O_3$ catalyst was located downstream the region II, O_3 and NO_2 outlet concentrations were reduced by approximately 97% and 89%, respectively. Plasma generated O_3 can be adsorbed on the catalyst surface and decomposed into active oxygen species, according to the following mechanism [45,46]:

$$O_3 + Z \rightarrow ZO + O_2 \quad (6)$$

$$O_3 + ZO \rightarrow Z + 2O_2 \quad (7)$$

where Z is active site on the catalyst surface. The decrease of NO_2 concentration in plasma-catalysis system can be attributed to the conversion of NO_2 to NO_3^- by the increasing amounts of active oxygen species. Devahasdin et al. [47] also reported that nitrate ions (NO_3^-) were detected on the catalyst surface during ozone decomposition reaction.

3.4. Effect of water vapor on degradation reaction performance

3.4.1. Catalytic activity evaluation in humid gas stream

The effect of water vapor on benzene degradation and CO_2 selectivity in PPC system with $Ag_{0.9}Ce_{0.1}/\gamma\text{-}Al_2O_3$ catalyst is presented in Fig. 9. The results show that adding a small amount of water

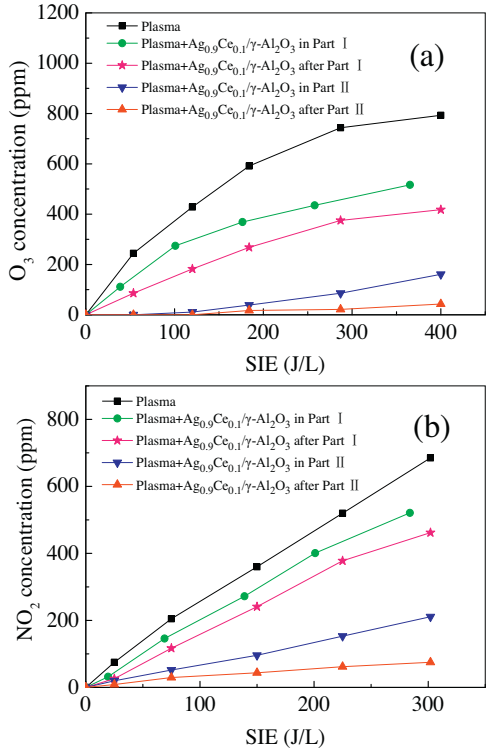

Fig. 8. Effect of plasma-catalysis configurations on (a) O_3 concentration and (b) NO_2 concentration as a function of *SIE*. Condition: $Ag_{0.9}Ce_{0.1}/\gamma$-Al_2O_3 was used as the catalyst, gas relative humidity was 0%.

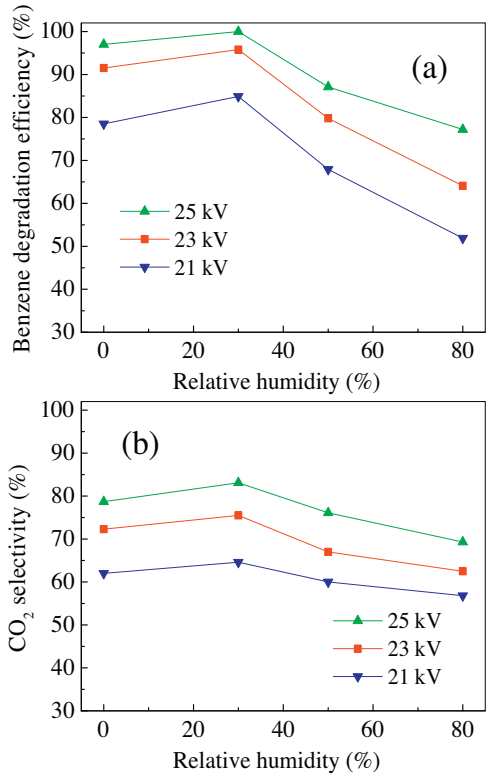

Fig. 9. Effect of gas relative humidity on (a) benzene degradation efficiency and (b) CO_2 selectivity as a function of *SIE*. Condition: the $Ag_{0.9}Ce_{0.1}/\gamma$-Al_2O_3 catalyst was placed downstream the region II.

vapor into plasma region enhances the catalyst activity in PPC system, and further increasing the gas relative humidity exhibits an obvious inhibiting effect. The benzene degradation efficiency and CO_2 selectivity enhanced from 97% and 78.7% to 100% and 83.1% as the gas relative humidity increased from 0 to 30% at 25 kV, while they greatly deceased to 77.2% and 69.3% at the relative humidity of 80%, respectively.

Water vapor could affect the benzene degradation in PPC process from the following aspects. Firstly, the presence of water vapor is considered to have significant impact on active species generation. A certain amount of water vapor could increase the amounts of •OH radicals and hydrogen atoms. However, as the gas relative humidity further increases, more energetic electrons could be quenched by electronegative water molecules, the electron density and average energy in discharge region would be decreased, resulting in a decrease of active species production. Secondly, the addition of water vapor can also change the discharge characteristics. When water vapor accumulated on the dielectric surface, the surface resistance decreased and the effective dielectric capacity increased, which lead to decline of total current in the system as well as the numbers of electrons [48]. Thirdly, excessive amount of water molecules would decrease the number of active sites available for benzene molecules and ozone adsorption due to the competitive adsorption of water molecules on active catalyst sites [49]. Besides, Einaga et al. [50] also found that the existence of water vapor in the ozone decomposition induced the structural changes of MnO_x/Al_2O_3 catalyst. Mn atom was oxidized to higher oxidation state with the coordination of H_2O to Mn site, which was caused by the cleavage of Mn—O—Al bond.

3.4.2. *Ozone and NO_x production in humid gas stream*

Fig. 10 shows the effect of water vapor on the formation of discharge byproducts O_3 and NO_2 in NTP system and PPC system with $Ag_{0.9}Ce_{0.1}/\gamma$-Al_2O_3 catalyst. The results in Fig. 10(a),(c) shows a decreasing O_3 concentration as the gas relative humidity increased for NTP process, but exhibits an increasing O_3 concentration for PPC process. This phenomenon indicates that the increase of gas relative humidity has an adverse effect on O_3 catalytic decomposition due to the competitive adsorption between H_2O and O_3 molecules. At the same time, the chemical reactions on catalyst surface, such as interaction between the adsorbed oxygen species and benzene as well as related organic intermediates were also suppressed at high gas relative humidity.

It is seen from Fig. 10(b),(d) that NO_2 outlet concentration decreases with the increase of gas relative humidity in both NTP and PPC systems. At 25 kV, the NO_2 concentration were 685 and 82 ppm for NTP and PPC systems in dry air, respectively, which decreased to 341 and 34.7 ppm at relative humidity of 80%. The decrease of NO_2 concentration in humid gas stream can be explained in two ways. Firstly, high gas relative humidity in discharge plasma tends to induce electron attachment reaction and thereby reduce the energetic electron density and mean electron energy, resulting in a decreased total production of active species. Secondly, the generation of •OH radical leads to a more efficient reaction with NO and NO_2 through the following possible reaction pathways [51,52]:

$$NO + {}^{\circ}OH + \rightarrow HNO_2 k = 3.3 \times 10^{-11} cm^3 molecule^{-1} s^{-1} \quad (8)$$

$$HNO_2 + {}^{\circ}OH + \rightarrow H_2O + NO_2 k = 6.0 \times 10^{-12} cm^3 molecule^{-1} s^{-1} \quad (9)$$

$$NO_2 + {}^{\circ}OH \rightarrow HO_2 + NO k = 7.7 \times 10^{-16} cm^3 molecule^{-1} s^{-1} \quad (10)$$

3.5. *Reaction by-products identification and degradation mechanism analysis*

Fig. 11 shows the FT-IR spectra of the effluent treated by NTP and PPC (system D) processes. The main gaseous products from

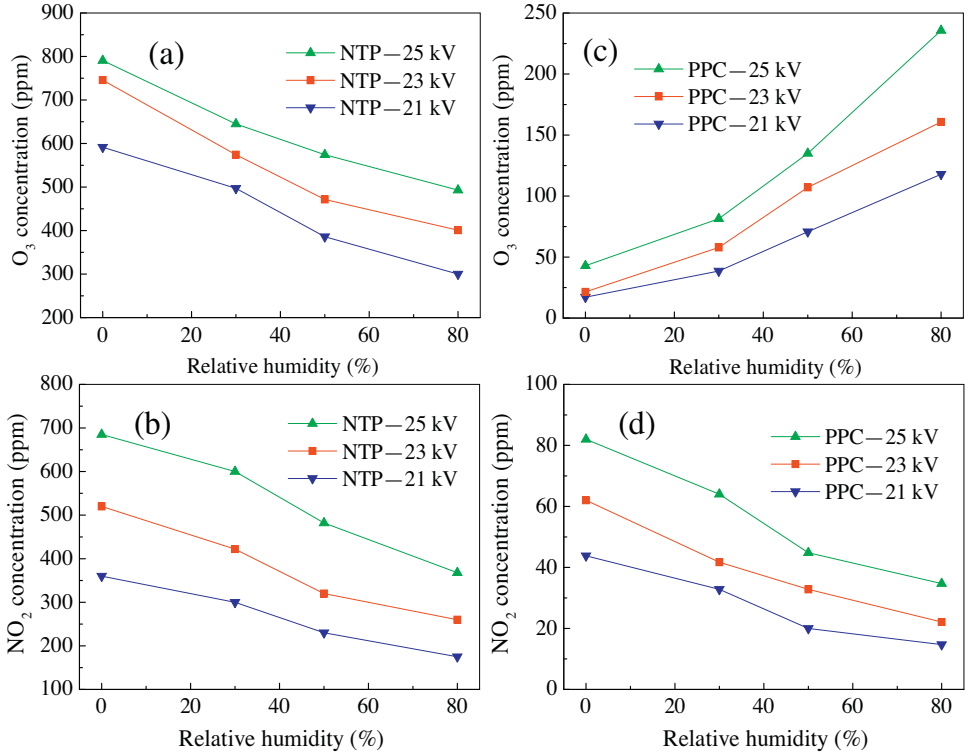

Fig. 10. Effect of gas relative humidity on the formation of O_3 and NO_2 as a function of *SIE* in NTP and PPC systems: (a) O_3 concentration in NTP system, (b) NO_2 concentration in NTP system, (c) O_3 concentration in PPC system, and (d) NO_2 concentration in PPC system. Condition: the $Ag_{0.9}Ce_{0.1}/\gamma\text{-}Al_2O_3$ catalyst was placed downstream the region II.

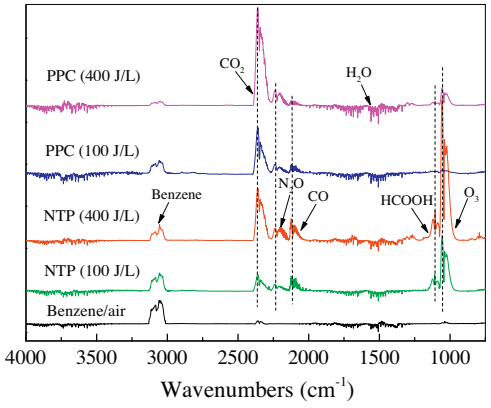

Fig. 11. FT-IR spectra of the gaseous products at the exit of the NTP and PPC systems between 700 and 4000 cm^{-1}.

NTP reactions were CO_2 and H_2O, with small amounts of CO and formic acid being also formed. Ozone and N_2O were also detected after the plasma processing. It is also clear that ozone is effectively decomposed on the surface of $Ag_{0.9}Ce_{0.1}/\gamma\text{-}Al_2O_3$ catalyst and most of benzene is converted into CO_2 in PPC process. The decreased adsorption peaks of formic acid and CO and the increased adsorption peaks of CO_2 and H_2O indicate that the hazardous intermediates can be further mineralized into the non-toxic products in PPC process over $Ag_{0.9}Ce_{0.1}/\gamma\text{-}Al_2O_3$ catalyst. In addition, some deposit was also accumulated on the surface of catalysts after long time (24 h) plasma-catalytic reaction at low *SIE* (100 J/L). The deposit was extracted with ethanol under ultrasonic vibration and analyzed by GC–MS, and the main components were identified as phenol, hydroquinone, heptanoic acid, 4-nitrocatechol, and 4-phenoxy-phenol.

Benzene decomposition in PPC process can be ascribed to both direct plasma reactions and plasma-catalytic surface reactions. The direct plasma reactions for the degradation of benzene are mainly induced by energetic electrons and plasma generated active species such as $^{\circ}O$, $^{\circ}N$, $^{\circ}OH$, $N_2\left(A^3\sum_u^+\right)$, etc. According to the organic intermediates analysis, hydroxylation products and organic acid are the main intermediates from the initial steps of benzene decomposition. These intermediates can be further oxidized by oxygenate active species such as $^{\bullet}O$ and $^{\bullet}OH$ to form final products CO_2 and H_2O. Plasma-catalytic surface reactions also contribute to the degradation of benzene. In PPC configuration where the $Ag_{0.9}Ce_{0.1}/\gamma\text{-}Al_2O_3$ catalyst are placed downstream the region II, both benzene molecules and intermediates generated from direct plasma reactions can be adsorbed on the catalyst surface. Subsequently, the benzene and intermediates molecules can be mainly oxidized into CO_2 and H_2O by active oxygen species generated on the catalyst surface via surface reactions, whilst the resultant oxygen vacancies could be replenished by gas phase oxygen and active oxygen species generated in NTP process. The alternative oxidation and reduction reactions of metal active sites on catalyst surface provide a continuous supply of active oxygen species as a rate-determining step.

4. Conclusion

In this study, we experimentally studied the degradation of benzene in IPC and PPC configurations, formed by a hybrid surface/packed-bed discharge (HSPBD) with different $Ag_x\,Ce_{1-x}/\gamma\text{-}Al_2O_3$ catalysts. The effects of Ag/Ce molar ratio, catalyst placement, and gas relative humid on the plasma-catalytic degradation of benzene have also been investigated.

The plasma-catalysis system led to an enhancement of benzene degradation compared to the plasma-only system, and which exhibited an obvious synergistic enhancement rather than a sim-

ple additive effect from the combination of plasma and catalysis. The $Ag_{0.9}Ce_{0.1}/\gamma$-Al_2O_3 catalyst showed the best catalytic activity for benzene degradation among all the catalysts with the highest degradation efficiency of 96.2% and CO_2 selectivity of 77.3% at the *SIE* of 400 J/L. The combination of Ag and Ce species with certain proportion facilitated the surface lattice of catalyst and increased the formation of surface adsorbed oxygen (O_{ads}), which played a key role in the plasma-catalytic reactions and significantly improved benzene degradation. Compared to IPC processes, PPC processes were found to be more effective at decomposing O_3 and destroying benzene due to the ability of catalysts to adequately decompose NTP generated ozone, especially when the catalysts were packed downstream the region II. Moreover, the presence of Ag_x Ce_{1-x}/γ-Al_2O_3 catalyst dramatically reduced the discharge products and gaseous hazardous intermediates. The change of gas relative humidity could affect the active species production and the activity of Ag_x Ce_{1-x}/γ-Al_2O_3 catalyst, and therefore there existed an appropriate gas relative humidity for benzene degradation.

Acknowledgments

This work is financially supported by the National Natural Science Foundation of China (No. 51177007 and No. 51507026).

References

[1] A.M. Vandenbroucke, M. Mora, C. Jiménez-Sanchidrián, F.J. Romero-Salguero, N. De Geyter, C. Leys, R. Morent, Appl. Catal. B 156–157 (2014) 94–109.
[2] X.M. Zhang, Y.F. Huang, Z. Liu, K.P. Yan, J. Electrostat. 76 (2015) 31–38.
[3] J.D. Coates, R. Chakraborty, J.G. Lack, S.M. O'Connor, K.A. Cole, K.S. Bender, L.A. Achenbach, Nature 411 (2001) 1039–1043.
[4] T. Shao, H. Jiang, C. Zhang, P. Yan, M.I. Lomaev, V.F. Tarasenko, Europhys. Lett. 101 (2013) 45002.
[5] J. Song, J. Tang, Y. Huo, Y. Wang, L. Wei, D. Yu, Phys. Plasma 21 (2014) 100704.
[6] T. Shao, V.F. Tarasenko, C. Zhang, E.K. Baksht, D. Zhang, M.V. Erofeev, C. Ren, Y.V. Shutko, P. Yan, J. Appl. Phys. 113 (2013) 093301.
[7] J. Song, J. Tang, Y. Wang, L. Wei, C. Ren, D. Yu, Phys. Plasma 22 (2015) 050703.
[8] R. Aerts, X. Tu, W.V. Gaens, J.C. Whitehead, A. Bogaerts, Environ. Sci. Technol. 47 (2013) 6478–6485.
[9] N. Jiang, N. Lu, K. Shang, J. Li, Y. Wu, Environ. Sci. Technol. 47 (2013) 9898–9903.
[10] B. Zhu, X.S. Li, J.L. Liu, J.B. Liu, X.B. Zhu, A.M. Zhu, Appl. Catal. B 179 (2015) 69–77.
[11] R. Morent, J. Dewulf, N. Steenhaut, C. Leys, H. Van Langenhove, J. Adv. Oxid. Technol. 9 (1) (2006) 53–58.
[12] M. Magureanu, N.B. Mandache, V.I. Parvulescu, C. Subrahmanyam, A. Renken, L. Kiwi- Minsker, Appl. Catal. B 74 (3–4) (2007) 270–277.
[13] X.B. Zhu, X. Gao, R. Qin, R.Y. Qu, C.H. Zheng, X. Tu, Appl. Catal. B 170–171 (2015) 293–300.
[14] X. Fan, T.L. Zhu, M.Y. Wang, X.M. Li, Chemosphere 75 (2009) 1301–1306.
[15] A.M. Harling, V. Demidyuk, S.J. Fischer, J.C. Whitehead, Appl. Catal. B: Environ. 82 (2008) 180–189.
[16] J.V. Durme, J. Dewulf, C. Leys, H. Van Langenhove, Appl. Catal. B Environ. 78 (2008) 324–333.
[17] A.M. Harling, D.J. Glover, J.C. Whitehead, K. Zhang, Appl. Catal. B 90 (2009) 157–160.
[18] C. Barakata, P. Gravejat, O. Guaitella, F. Thevenet, A. Rousseau, Appl. Catal. B 147 (2014) 302–313.
[19] A. Maciuca, C. Batiot-Dupeyrat, J.M. Tatibouët, Appl. Catal. B 125 (2012) 432–438.
[20] J. Jarrige, P. Vervisch, Appl. Catal. B 90 (2009) 74–82.
[21] H.T. An, T.P. Huu, T.L. Van, J.M. Cormier, A. Khacef, Catal. Today 176 (2011) 474–477.
[22] M. Magureanua, D. Piroia, N.B. Mandachea, V.I. Pârvulescub, V. Pârvulescuc, B. Cojocarub, C. Cadigand, R. Richardsd, H. Dalye, C. Hardacree, Appl. Catal. B 104 (2011) 84–90.
[23] J. Karuppiah, L. Sivachandiran, R. Karvembu, Ch. Subrahmanyam, Chem. Eng. J. 165 (2010) 194–199.
[24] H.H. Kim, Y. Teramoto, T. Sano, N. Negishi, A. Ogata, Appl. Catal. B 166–167 (2015) 9–17.
[25] M.T. Nguyen Dinh, J.M. Giraudon, A.M. Vandenbroucke, R. Morent, N. De Geyter, J.F. Lamonier, Appl. Catal. B 172 (2015) 65–72.
[26] Q.H. Trinh, S.B. Lee, Y.S. Mok, J. Hazard. Mater. 285 (2015) 525–534.
[27] X.J. Tang, F.D. Feng, L.L. Ye, X.M. Zhang, Y.F. Huang, Z. Liu, K.P. Yan, Catal. Today 211 (2013) 39–43.
[28] H. Einaga, A. Ogata, Environ. Sci. Technol. 44 (2010) 2612–2617.
[29] H.J. Sedjame, C. Fontaine, G. Lafaye, J. Barbier Jr., Appl. Catal. B 144 (2014) 233–242.
[30] C.Y. Ma, D.H. Wang, W.J. Xue, B.J. Dou, H.L. Wang, Z.P. Hao, Environ. Sci. Technol. 45 (2011) 3628–3634.
[31] H.X. Ding, A.M. Zhu, F.G. Lu, Y. Xu, J. Zhang, X.F. Yang, J. Phys. D Appl. Phys. 39 (2006) 3603–3608.
[32] K. Yamazaki, T. Kayama, F. Dong, H. Shinjoh, J. Catal. 282 (2011) 289–298.
[33] C. Subrahmanyam, M. Magureanu, A. Renken, L.K. Minsker, Appl. Catal. B 65 (2006) 150–156.
[34] W.J. Liang, J. Li, J. Li, Y.Q. Jin, J. Hazard. Mater. 170 (2009) 633–638.
[35] T. Xing, H.Q. Wan, Y. Shao, Y.X. Han, Z.Y. Xu, S.R. Zheng, Appl. Catal. A 468 (2013) 269–275.
[36] Z.Y. Ji, X.P. Shen, G.X. Yang, Appl. Catal. B 144 (2014) 454–461.
[37] K. Yamazaki, T. Kayama, F. Dong, H. Shinjoh, J. Catal. 282 (2011) 289–298.
[38] W. Teng, X.Y. Li, Q.D. Zhao, J.J. Zhao, D.K. Zhang, Appl. Catal. B 125 (2012) 538–545.
[39] P. Burroughs, A. Hamnett, A.F. Orchard, G. Thornton, J. Chem. Soc. Dalton Trans. 17 (1976) 1686–1698.
[40] F. Zhang, P. Wang, J. Koberstein, S. Khalid, S. Chan, Surf. Sci. 563 (2004) 74–82.
[41] Z. Qu, F. Yu, X. Zhang, Y. Wang, J. Gao, Chem. Eng. J. 229 (2013) 522–532.
[42] G. Zhou, H. Lan, T. Gao, H. Xie, Chem. Eng. J. 246 (2014) 53–63.
[43] A. Ogata, D. Ito, K. Mizuno, S. Kushiyama, T. Yamamoto, IEEE Trans. Ind. Appl. 37 (2001) 959–964.
[44] X. Tu, J.C. Whitehead, Appl. Catal. B 125 (2012) 439–448.
[45] W. Li, S.T. Oyama, J. Am. Chem. Soc. 120 (1998) 9047–9052.
[46] V. Demidyuk, J.C. Whitehead, Plasma Chem. Plasma Process 27 (2007) 85–94.
[47] S. Devashasdin, C. Fan, J.K. Li, D.H. Chen, J. Photochem. Photobiol. A 156 (2003) 161–170.
[48] Z. Falkenstein, J.J. Coogan, J. Phys. D Appl. Phys. 30 (1997) 817–825.
[49] J.L. Wu, Q.B. Xia, H.H. Wang, Z. Li, Appl. Catal. B 156–157 (2014) 265–272.
[50] H. Eigaga, M. Harada, S. Futamura, Chem. Phys. Lett. 408 (2005) 377–380.
[51] R. Atkinson, D.L. Baulch, R.A. Cox, J.N. Crowley, R.F. Hampson, R.G. Hynes, M.E. Jenkin, M.J. Rossi, J. Troe, J. Phys. Chem. Ref. Data 21 (1992) 1125–1568.
[52] W. Tsang, J.T. Herron, J. Phys. Chem. Ref. Data 20 (1991) 609–663.